

Multi-Exposure Image Fusion via Distilled 3D LUT Grid with Editable Mode

Xin Su¹, and Zhuoran Zheng^{2*}, *Member, IEEE*
¹ Fuzhou University, ² Sun Yat-sen University

Abstract—With the rising imaging resolution of handheld devices, existing multi-exposure image fusion algorithms struggle to generate a high dynamic range image with ultra-high resolution in real-time. Apart from that, there is a trend to design a manageable and editable algorithm as the different needs of real application scenarios. To tackle these issues, we introduce 3D LUT technology, which can enhance images with ultra-high-definition (UHD) resolution in real time on resource-constrained devices. However, since the fusion of information from multiple images with different exposure rates is uncertain, and this uncertainty significantly trials the generalization power of the 3D LUT grid. To address this issue and ensure a robust learning space for the model, we propose using a teacher-student network to model the uncertainty on the 3D LUT grid. Furthermore, we provide an editable mode for the multi-exposure image fusion algorithm by using the implicit representation function to match the requirements in different scenarios. Extensive experiments demonstrate that our proposed method is highly competitive in efficiency and accuracy. The code is released at <https://github.com/zxr-idam/UHD-multi-exposure-image-fusion-algorithm>.

Index Terms—Multi-exposure image fusion, 3D LUT technology, ultra-high-definition, teacher-student network, implicit representation function.

I. INTRODUCTION

To boost the dynamic range of natural images recorded by handheld devices, Multi-Exposure image Fusion (MEF) techniques [8], [10], [14], [22], [23], [32], [33], [35], [38], [44], [45] are widely employed to generate a visually pleasing image. Recently, with the continuous development and improvement of hardware technology, photos or videos from handheld devices can usually be recorded with ultra-high-definition (UHD) resolution. Despite the advantages of UHD resolution, the high density of pixels (in the millions) can cause existing Multi-Exposure Fusion (MEF) algorithms to fail when running on resource-limited devices. This is particularly true for deep learning approaches such as a simple CNN with three layers of convolution, where fusion of more than 3 UHD images with differing exposures at once could cause the CPU on a mobile phone to be unable to handle the workload. Apart from the aforementioned limitation, current MEF algorithms also lack customization options to cater to unique demands of different scenarios.

Faced with the limitations of these MEF algorithms, our research explores general techniques for enhancing UHD images. So far, there are three mainstream deep learning-based solutions: 1) Bilateral learning [46]; 2) 3D LUT [41]; and 3) Laplace pyramid [30]. All of these methods are designed to speed up the process of enhancing UHD images with different



Fig. 1. The top figure shows the results of our method run on a multi-exposure dataset. **Size** illustrates the scale of the 3D LUT grid, for example, 32 means the size of the grid is $32 \times 32 \times 32$, and the PSNR is gradually increased with the size of the grid. Note that the scale of this grid is editable due to our use of implicit neural representation. The bottom figure shows the average running time comparison over MEFB, a dataset containing 50 image pairs of average size $3 \times 551 \times 707$.

resolutions. Notably, the 3D LUT-based algorithm can process a 4K image in just 9ms on a single GPU. This is made possible by incorporating prior knowledge of image retouching techniques. The algorithm pre-designs several toned grids and uses a deep network to learn the weights of these grids for fusion. Finally, the fused grids are applied to the raw image for enhancement. To trade-off the accuracy and efficiency of the regression, here we select a 3D LUT-based deep learning method as a base to generate a high dynamic range (HDR) image with UHD resolution. Although 3D LUT has the potential to handle UHD MEF tasks, existing 3D LUT techniques only enhance a single input image, and we need to address the following concerns when faced with a set of the input image. **i)** How to generate a robust grid acting on the raw information when faced with multiple images whose luminance, texture, and color are different (facing the issue of information fusion with **uncertainty**). **ii)** In addition, on which **raw information** (synthetic information or an raw image)

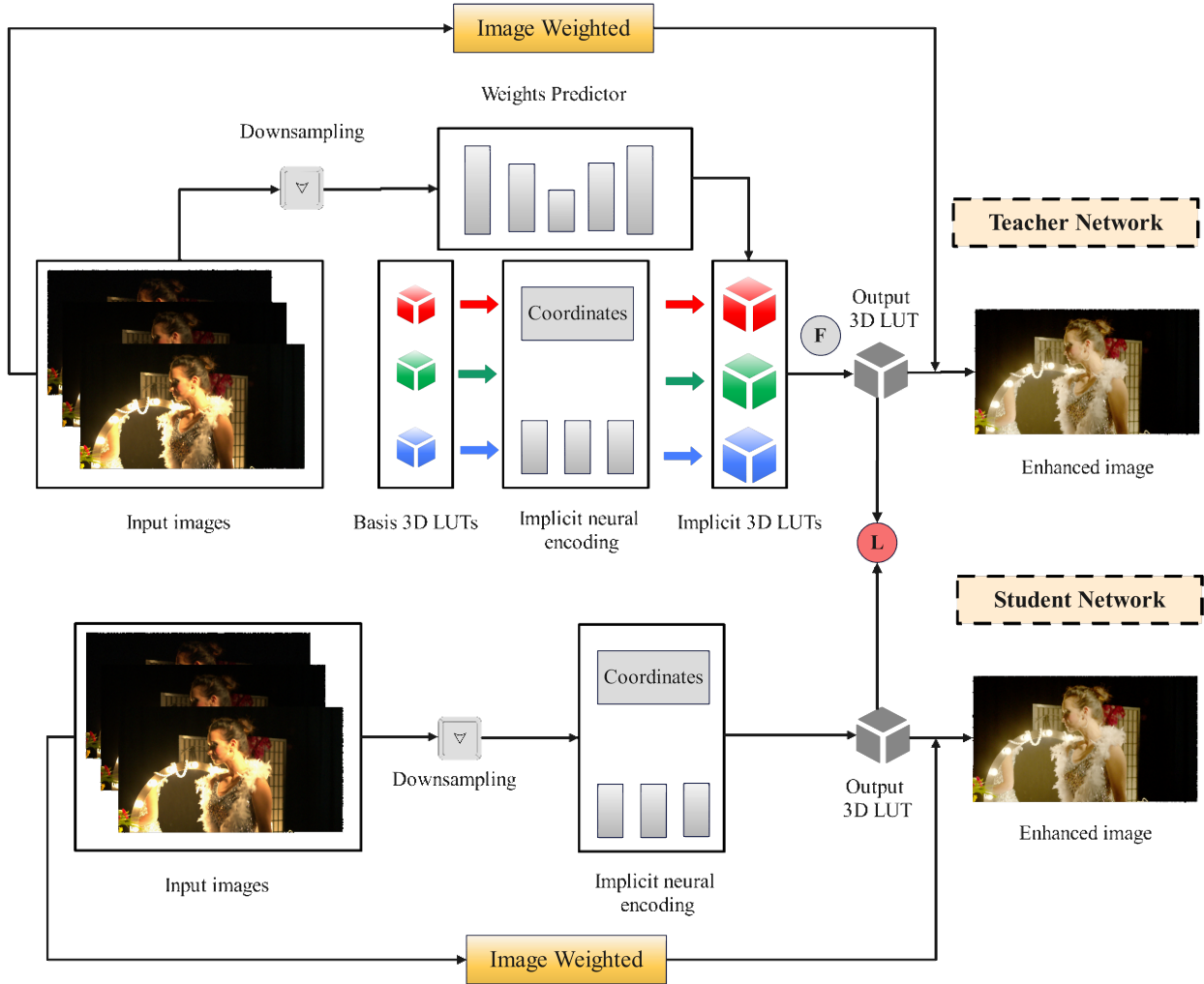


Fig. 2. **The architecture of our approach.** This figure shows a learning paradigm for a student-teacher network. First, the teacher network learns a high-quality 3D LUT, after that, the 3D LUT in the student network is constrained by the teacher network, and finally, the student network generates a robust 3D LUT. **F** denotes the weighted fusion strategy and **L** denotes the restricted loss term.

should the grid act? **iii)** How to extend this technology into a customized algorithm that is manageable and editable?

To tackle these issues, we develop a method that leverages a teacher-student network to build a distilled 3D LUT grid for fusing a set of low dynamic range images [37]. Specifically, we constrain the 3D LUT grid to model the uncertainty of the input information by encoding the correlation between the patch of true image and then selecting the raw images to be enhanced with the help of a classifier (a small-scale CNN with MLP). The whole 3D LUT encoder is modeled by an implicit neural network (student network) [20], which is an editable pattern to generate high dynamic range images of varying quality. Our approach employs a lightweight network that can process 5 UHD resolution images on a single GPU, achieving real-time processing speed of at least 33fps. In our experimental section, we evaluate the algorithm using several publicly available datasets as well as a customized dataset. Results from a large number of experiments demonstrate the effectiveness of our approach.

The contributions of this paper are summarized as follows:

- We propose a teacher-student network architecture for

learning to a distilled 3D LUT grid, which boosts the generalization ability of the student network by modeling uncertainty.

- We introduce an implicit neural network to build a student network to yield a 3D LUT grid of arbitrary size, which can be used to generate UHD images of different quality based on the scene conditions.
- By discussing and experimenting to bridge the gap between the three popular UHD degradation image enhancement methods, in addition, a large number of experiments (quantitative and qualitative evaluations) demonstrate the effectiveness of our approach.

II. RELATED WORK

Image fusion methods. Conventional methods for image fusion include spatial domain-based methods and transformation domain-based algorithms. Spatial domain approaches [7], [16], [17] analyze the information significance of raw images and fuse them spatially using an estimated weight map. On the other hand, transformation domain approaches [9] concentrate on the coefficients of decomposed basis vectors and assess the

importance of these signals by using a simple model before fusion.

Recently, deep learning-based approaches have delivered promising results in the MEF field. Based on the convolutional neural network (CNN), Deepfuse [23] first proposes that the merging of luminance maps is represented by deep learning and fuses chromaticity different parts by conventional weighted averaging methods. Subsequently, a large number of CNN-based approaches are proposed, such as those based on generative adversarial networks [19]. However, these methods are a local modeling strategy and they struggle to capture the global information of the image, and to solve this problem, Transformer-based methods are proposed. Although these methods are demonstrated to be effective on MEF tasks, they usually require stacking a large number of convolutional layers and attention modules, which can yield artifacts or ghost motifs easily in real scenes. In addition, unsupervised and self-supervised based methods have been heavily introduced to alleviate the problems of unpaired images and over-fitting. Most of the above models cannot directly process 4K or higher resolution images on a single GPU shader with 24G RAM.

LUTs for image enhancement. 3D look-up tables (LUTs) are ultra-fast algorithms for color mapping and are widely used to improve the quality of digital images for color correction, video enhancement, and retouching. In recent years, many neural network-based LUT generation methods are proposed [6], [36], [40], [42]. Image-Adaptive 3DLUT uses a simple CNN weight predictor to estimate several basic 3D LUT weights learned. Then, an adaptive 3D LUT is generated for each input image based on the image content fusion 3D LUT. Afterwards, the 3D LUTs are fused to generate a grid containing the affine transform coefficients, and finally this grid acts on the raw image to achieve image enhancement. 4D LUT proposes a context-aware 4D lookup table that can be adapted to learn the photo context to achieve content-dependent enhancement of different contents in each image. CLUT analyses the inherent compressibility of 3D LUT and proposes an efficient 3D LUT compression representation that maintains the powerful mapping capability of 3D LUT. These methods explore the use of neural networks to generate LUTs, showing the robust capabilities of LUTs in image and video processing.

UHD image processing methods. To transfer our laboratory models to real application scenarios effectively, HD image research [4], [25]–[29], [39], [43] which can be processed in real-time is becoming popular. After that, with the development of deep learning techniques, some methods for real-time processing of UHD images are proposed. However, at present, the method for UHD multi-exposure image processing is still in a limbo stage.

III. METHOD

The workflow of our approach is illustrated in Figure 2 (best viewed in color). Through a distillation loss $\mathcal{L}_{\text{grid}}$ bridges the teacher network and the student network; it can be noticed that the student network does not with customized 3D LUTs, rather it just regresses a cubic grid using an implicit neural network. Our approach is depicted by five sub-summaries.

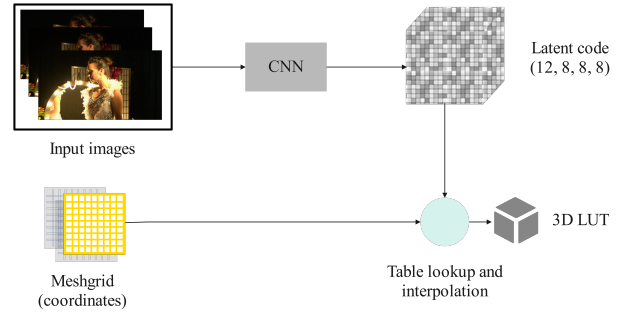


Fig. 3. The architecture of implicit neural network.

Generating a 3D lookup tables. In this paper, we view a 3D LUT as an implicit neural network regression target (student network), which is a continuous space where the size of the grid is in **editable mode**. In a nutshell, an implicit neural network \mathbf{F}_{INN} receives a pair of information (latent code l and coordinates c) that can be regressed to the element e corresponding to that coordinate value. Here the latent code l is a feature map by a lightweight CNN encoding the input information, here is a feature map of size $12 \times 8 \times 8 \times 8$. The coordinates c are in editable mode and the dimensions can be generated arbitrarily. The whole flow is shown in Figure 3, where the table lookup and interpolation use https://pytorch.org/docs/stable/generated/torch.nn.functional.grid_sample.html#torch.nn.functional.grid_sample. This process can be written as

$$v_{(i,j,k)} = \mathbf{F}_{\text{INN}}(l, c(i, j, k)), \quad (1)$$

where i, j, k denotes the coordinates on the three-dimensional space, v denotes the element at each position in the 3D LUT V . Finally, the 3D LUT grid V acts on a given raw information (qualified by a network) to generate an enhanced image. For the teacher network, to fuse a high-quality grid \hat{V} needs to input three prior grids ($V1 = \{v1_r, v1_g, v1_b\}$, $V2 = \{v2_r, v2_g, v2_b\}$, $V3 = \{v3_r, v3_g, v3_b\}$) into a simple CNN to generate three $\{L_1, L_2, L_3\}$; after that, they are input to the implicit neural network \mathbf{F}_{INFF} to obtain three enhanced grids ($\hat{V}_1, \hat{V}_2, \hat{V}_3$); finally, they are predicted by Weights Predictor (WP) to conduct a linear fusion of the three weights (w_1, w_2, w_3). WP is a lightweight CNN that predicts a set of weights from the input images.

Teacher network. The teacher network can be viewed as a standard 3D LUT model, where the only concern is simply the information input from multiple images I_* . Specifically, the primary issue to consider is computational efficiency. To obtain fast inference capability, the extant methods for handling UHD images require large-scale downsampling of the raw input ($3840 \times 2160 \rightarrow 256 \times 256$). Here, we downsample the resolution of the raw images to 128×128 . Then, the I_* 's are stacked in the channel dimension \mathbb{C} , following a sequence of gradually growing exposure. The input information that is pre-processed then passes to two networks (IW [Image Weighted], WP [Weights Predictor]). WP aims to provide weights for fusing 3D LUTs V . WP is a U-Net network [24] with several layers of MLPs, and the number of neurons in the last layer

of MLPs corresponds to the number of basis 3D LUTs.

$$w_* = \text{WP}(\text{S}(I_*)), \quad (2)$$

where S denotes that the images are stacked on the channel domain \mathbb{C} . The IW aims to provide a high-quality reconstruction target for \hat{V} , which feeds the input images with the weights required for fusion. IW utilizes only several 3×3 convolutions and two layers of MLP, with the last layer being Softmax . This algorithm can be formalized as follows

$$I_f = \text{IW}(\text{S}(I_*)) \cdot \mathbf{I}, \quad (3)$$

where I_f represents the fused image and \mathbf{I} represent a set of multi-exposure images with the original resolution. In general, the whole inference process of the teacher network can be written

$$I_E = \hat{V} \Delta I_f, \quad (4)$$

where I_E represents the obtained UHD-enhanced image and Δ represents trilinear interpolation and lookup scheme.

Student network. The student network is a **lightweight network** that does not rely on any prior knowledge and regresses a 3D LUT grid through a set of networks (IW and implicit neural network). The overall workflow can be written

$$I_E = V \Delta I_f, \quad (5)$$

Loss functions. The key to our approach lies in the design of the loss function. For the teacher network, we use only one \mathbf{L}_1 loss, which focuses on the difference between each pixel value. For the student network, we need to trade off the three loss function terms to generate a robust 3D LUT grid V . Specifically, the first is the \mathbf{L}_1 loss function, which computes the distance between I_E (output of the algorithm) and the truth image I_G . The second loss term \mathcal{L}_{d1} is the distillation loss about grid V . The distance between $V \in \mathbb{R}^{64 \times 64 \times 64}$ and $\hat{V} \in \mathbb{R}^{64 \times 64 \times 64}$ is measured through an \mathbf{L}_1 loss. The third loss term \mathcal{L}_{lr} aims to boost the robustness of the student network, and it has the assumption that the long-range dependencies between the elements of the grid should be similar to I_G . Specifically, I_G is tokenized (similar to ViT [3]’s serialization step) and then gets a correlation matrix $\mathcal{M}_g \in \mathbb{R}^{16 \times 16}$ between image patches by the dot product. V is tokenized through a small CNN network to obtain a matrix $\mathcal{M}_b \in \mathbb{R}^{16 \times 16}$. The assumption of \mathcal{L}_{lr} is based on our observations of the data distribution of each of V and I_G . This assumption is explored in the discussion section. The total loss function $\mathcal{L}_{\text{total}}$ can be written

$$\mathcal{L}_{\text{total}} = \mathcal{L}_1 + \alpha \mathcal{L}_{d1} + \beta \mathcal{L}_{lr}, \quad (6)$$

where α and β were set to 0.05 and 0.09, respectively; in addition, we also try to enforce a perceptual loss [5] on the student network, but the visual effect is not significant.

Details of the neural network. For the teacher network, the implicit neural coding comes with two sub-networks, where the CNN is a 5+2 network (5 convolutional layers with 3×3 convolutional kernels, the activation function uses ReLU); the MLP has only 5 layers (the activation function uses ELU). For the student network, the implicit neural coding comes with two sub-networks, where the CNN is an 8+2 network

(8 convolutional layers with 3×3 convolutional kernels, the activation function uses ReLU); the MLP has only 7 layers (the activation function uses ELU). IW employs a 3-layer convolution with a 2-layer MLP, and the activation function uses ReLU. In addition, to generate matrix \mathcal{M}_b , the customized CNN network employs 5 convolutional layers with 3×3 convolutional kernels. To tokenize I_G , we use a CNN stem, which is just a convolutional layer with a large-scale convolution kernel (16×16).

IV. EXPERIMENTS

We introduce a set of experiments to evaluate and analyze the effectiveness of our proposed method. In addition, we create a large dataset (**Multi-exposure Document Datasets**) with UHD resolution (resolution greater than 4K).

Dataset. We evaluate the algorithm on the *SICE* [1] and *NTIRE workshop22 Multi-frame HDR* [21] datasets. Each of the two datasets with 30% of the samples serves as the test set. Each scenario in the dataset includes three LDR images with various exposure levels (short/medium/long exposure). Moreover, since document recognition and detection is a very important application, a multi-exposure document dataset (MED) with UHD resolution is created for this purpose. Each document contains a pair of time-aligned short-exposure and long-exposure images and their corresponding ground truth. The underexposed and overexposed images of the document image can be formulated as follows according to the method proposed by Lv et al. [15] :

$$I_{out}^{(i)} = \beta \times (\alpha \times I_{in}^{(i)})^\gamma, i \in \{R, G, B\}, \quad (7)$$

where α and β are linear transformations, the X^γ (denotes all pixels in an image) means the gamma transformation. The three parameters are sampled from the uniform distribution \mathbb{U} : $\alpha \sim \mathbb{U}(0.9, 1)$, $\beta \sim \mathbb{U}(0.5, 1)$, $\gamma \sim \mathbb{U}(1.5, 5)$. However, this customized manner of building images is difficult to meet complex environmental transformations, such as blur, and noise. To tackle this problem, we attempt to employ CycleGAN [18] to enforce the noise of the environment on the synthesized dataset. The unpaired image dataset uses *SICE* (short/long images). We utilize an AdamW optimizer with an initial learning rate of 0.001 and train the CycleGAN for 100 epochs, delaying the learning rate by 0.1 after 50 and 75 epochs. Since CycleGAN may over-modify some images, such as generating dark corners, ghost textures, and other problems, we use adobe photoshop to repair them. Note that we do not employ professional devices for multi-exposure image synthesis for two reasons: i) existing devices cannot meet resolutions above 6K; ii) UHD images are difficult to align in the time dimension. Our document dataset includes contracts, papers, invoices, and other types, with a total of 1000 sets of images.

Implementation details. In the training phase, three input images with different exposure levels are divided into 1000×1000 resolution (bilinear interpolation or center cropping approach). The network is optimized by an AdamW optimizer with initial learning rate of $1e-4$ and decay rate of 0.1, we set $\beta_1 = 0.9$, $\beta_2 = 0.999$ and $\varepsilon = 10^{-8}$. Our network is

TABLE I
WE COMPARE SSIM AND PSNR INDICATORS ON THREE DATASETS RESPECTIVELY. IN ADDITION, WE STATISTICS THE NUMBER OF PARAMETERS OF THE MODELS. OUR METHOD CONTAINS ONLY 0.52M PARAMETERS.

Dataset	Metrics	Short	Medium	Long	HALDER(-)	AGAL(24M)	AHDR(1.44M)	U2fusion(-)	ADNet(2.80M)	Ours(0.52M)
SICE	PSNR	6.68	11.52	14.7	19.8	18.84	18.2	16.9	21.23	23.8
	SSIM	0.13	0.59	0.74	0.82	0.83	0.71	0.79	0.82	0.81
NTIRE22	PSNR	13.50	34.2	15.09	35.33	26.57	35.11	30.2	35.78	36.85
	SSIM	0.49	0.83	0.69	0.85	0.69	0.92	0.61	0.93	0.95
MED	PSNR	4.24	-	10.28	19.31	18.22	27.14	25.31	26.88	29.78
	SSIM	0.08	-	0.42	0.71	0.69	0.92	0.85	0.94	0.97



Fig. 4. Our method obtains better visual quality and recovers more image details compared with other state-of-the-art methods in the SICE datasets.

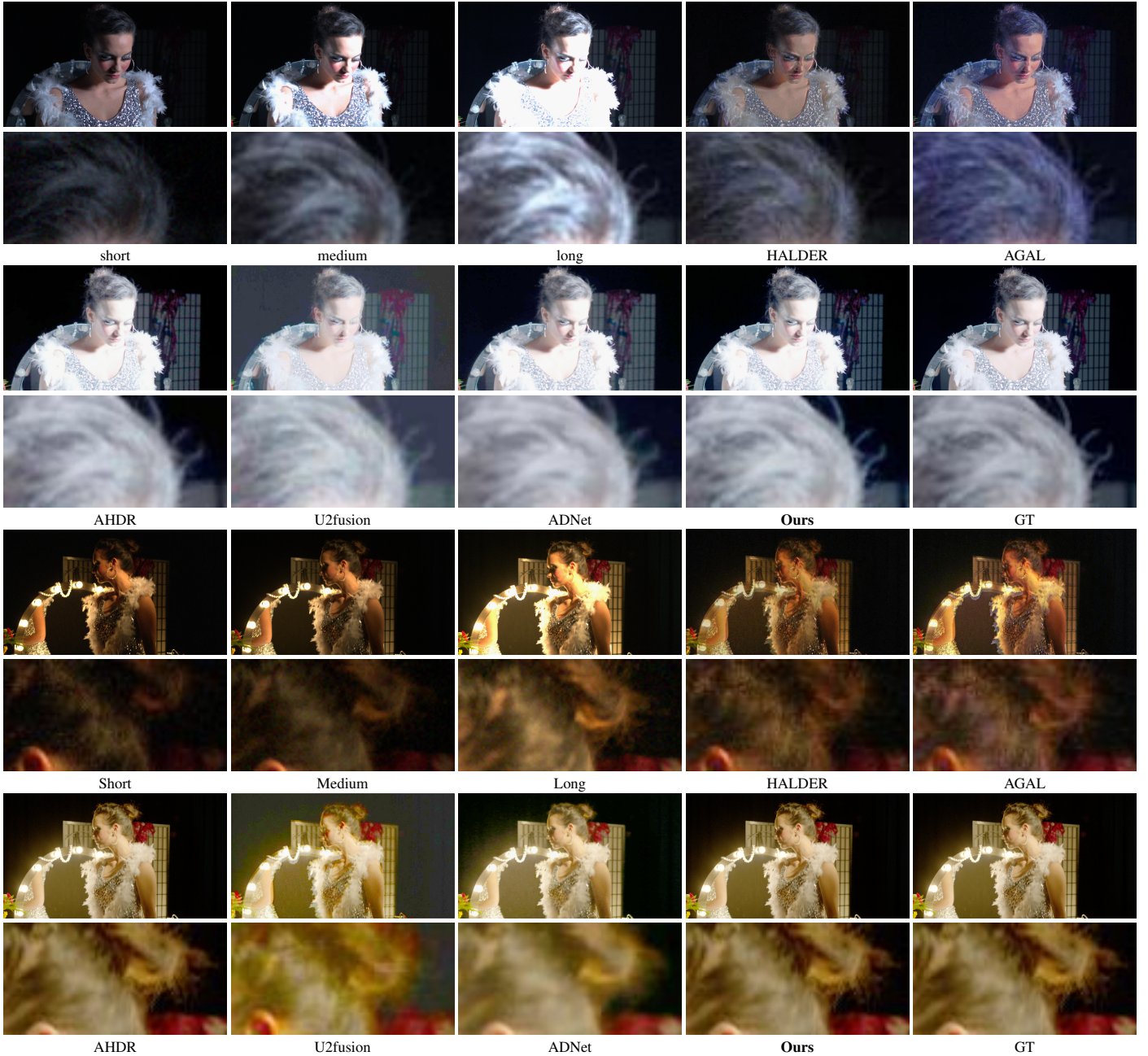


Fig. 5. Our method obtains better visual quality and more image details compared with other state-of-the-art methods in the NTIRE22 HDR datasets.

implemented on PyTorch 1.7, Koinra, and Python 3.8. Our whole training process is implemented on RTX3090 GPU shader with 24G RAM. The comparison algorithm is fine-tuned on all three datasets, and since these models do not have a customized lightweight design, the images are cropped to 512×512 during the training phase. These networks are optimized by an AdamW optimizer with initial learning rate of $1e-3$ and decay rate of 0.1, we set $\beta_1 = 0.9$, $\beta_2 = 0.999$ and $\varepsilon = 10^{-8}$. These comparison algorithms use a loss function that is an elaborate design for fine-tuning these three data sets. Here, first, we select to use MEF-SSIM loss based on unreferenced metric method [2] to conduct semi-supervised training. We used $I_k, k \in \{1, 2, 3\}$ to represent three input images with different exposure levels and used I_p to represent

the HDR image the model predicted.

$$\begin{aligned}
 I_k &= \|I_k - \mu_{I_k}\| \cdot \frac{I_k - \mu_{I_k}}{\|I_k - \mu_{I_k}\|} + \mu_{I_k} \\
 &= c_k \cdot s_k + l_k,
 \end{aligned} \tag{8}$$

where $\|\cdot\|$ is the \mathcal{L}_2 norm of pixel, μ_k is the mean value of I_k and \tilde{I}_k is the mean subtracted patch. The structure of the desired result (\hat{s}) is obtained by a weighted sum of structures of input patches. In addition, the desired contrast value \hat{c} can be represented as follows:

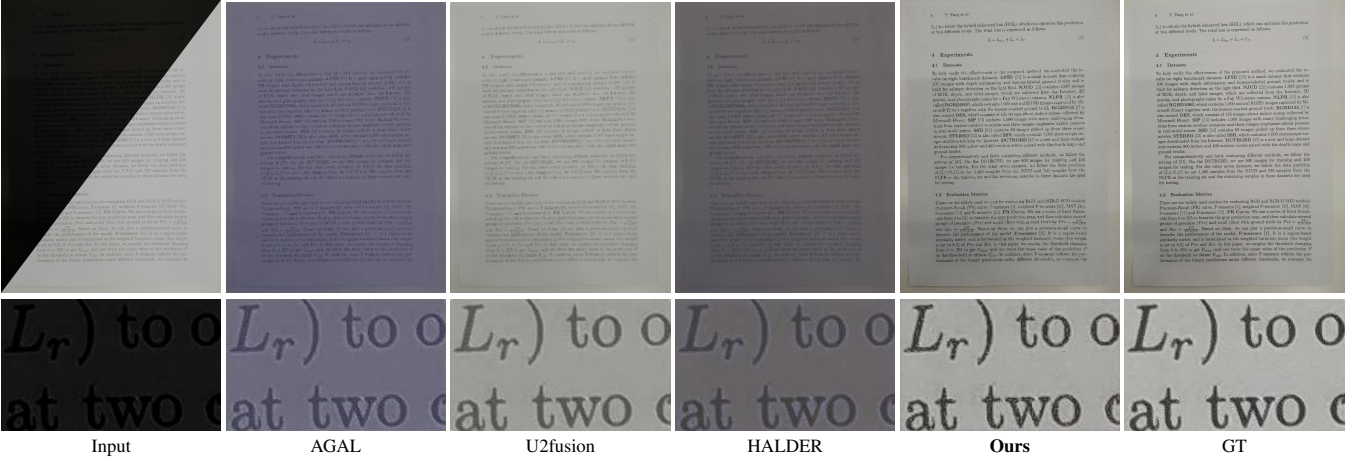


Fig. 6. Our method obtains better visual quality and recovers more image details compared with other state-of-the-art methods in the MED dataset.



Fig. 7. We select two groups of patches (local area of the image). The architecture of the teacher-student network can provide a clearer texture for the images inferred by the student network.



Fig. 8. We select two groups of patches (local area of the image). The architecture of the L_{Lr} can provide a clearer texture for the images inferred by the student network.

$$\begin{aligned} \hat{c} &= \max\{c_k\}, \\ \bar{s} &= \frac{\sum_{k=1}^2 w(\tilde{I}_k) s_k}{\sum_{k=1}^2 w(\tilde{I}_k)} \quad \text{and} \quad \hat{s} = \frac{\bar{s}}{\|\bar{s}\|}, \\ \hat{I} &= \hat{c} \cdot \hat{s}, \end{aligned} \quad (9)$$

where the \hat{I} stands for the result. The final image quality score for pixel p is calculated using the SSIM framework:

$$\text{Score}(p) = \frac{2\sigma_{\hat{I}_p} + C}{\sigma_{\hat{I}}^2 + \sigma_{I_p}^2 + C}, \quad (10)$$

where $\sigma_{\hat{I}}^2$ is variance and $\sigma_{\hat{I}_p}$ is covariance between \hat{I} and I_p

and the final loss is calculated as follows:

$$\mathcal{L}_t = 1 - \frac{1}{N} \sum_{p \in P} \text{Score}(p), \quad (11)$$

where N is the total number of pixels in the input image and P are the set of all pixels in the input image. In addition, we used traditional \mathcal{L}_1 to train for paired datasets. Therefore, our total loss can be expressed as follows:

$$L_{\text{total}} = \lambda_1 L_{\text{paired}} + \lambda_2 L_{\text{unpaired}}, \quad (12)$$

where λ_1 and λ_2 represent the weight of paired and unpaired data loss and we set the λ_1 0.9 and the λ_2 0.1. In addition, since AHDR [34] and ADNet [13] cannot run MED directly

TABLE II
QUANTIFIED RESULTS OF ABLATION EXPERIMENTS FOR NETWORK COMPONENTS. TN DENOTES TEACHER NETWORK.

Datasets	w/o TN		w/o \mathcal{L}_{lr}		Ours	
	PSNR	SSIM	PSNR	SSIM	PSNR	SSIM
SICE	21.22	0.72	23.6	0.80	23.8	0.81
MED	25.69	0.89	27.2	0.94	29.78	0.97

TABLE III
THE EFFECT OF DIFFERENT SIZES OF 3D LUT GRIDS ON RECONSTRUCTED IMAGES IN STUDENT NETWORKS.

	8	16	32	64	128
PSNR	15.4	22.1	23.8	24.1	24.2
SSIM	0.61	0.77	0.81	0.85	0.85

on a single GPU, for this reason, we sub-patch the images into the model before stitching.

Algorithm comparison. We compared our method with HALDER [11], AGAL [12], AHDR [34], U2fusion [31], ADNet [13] on SICE [1] dataset and the NTIRE workshop22 Multi-frame HDR dataset. Figure 4 shows two examples from the SICE dataset, Figure 5 shows two examples from NTIRE workshop22 Multi-frame HDR dataset and Figure 6 shows an example from MED. Through the demonstration of the samples, we find that U2fusion can generate artifacts when fusing images, this is because the unsupervised method is not stable. AGAL’s attention mechanism is more focused on fusing the textures of the images, while the colors are generally distorted. AdNet over-smoothed the texture. As shown in Table I, we evaluate the performance of the algorithm in terms of quantitative aspects, and in general, our method reaches the best in terms of speed and accuracy.

Ablation study. We conduct some ablation experiments to evaluate the effectiveness of the modules of our method. 1) **Effectiveness of teacher-student network.** We remove the teacher network and use only the student network to fuse the multi-exposure images. These networks are optimized by an AdamW optimizer with an initial learning rate of $1e-5$ and a decay rate of 0.1, we set $\beta_1 = 0.9$, $\beta_2 = 0.999$ and $\varepsilon = 10^{-8}$. For the loss function term, we use \mathcal{L}_1 and perceptual loss. As shown in Figure 7, our method provides clearer textures when reconstructing the local information of the image. 2) **Effectiveness of \mathcal{L}_{lr} .** We remove the loss function term \mathcal{L}_{lr} with the correlation between patches. As shown in Figure 7, our method provides clearer textures when reconstructing the local information of the image. 3) **Effectiveness of 3D LUT grid.** Our proposed implicit neural network can be run in edit mode to generate a 3D LUT grid of arbitrary size, and here we evaluate the role of different scale grids on the SICE dataset (see Table III). We observe an optimal trade-off between speed and accuracy when the grid size reaches 32. In addition to these, we quantitatively evaluate the ablation experiments on the SICE and MED dataset (see Table II).

Deployment of mobile devices. We also deploy our proposed network on Android virtual mobile (102ms) and Raspberry PI (89ms) for the real-time image processing requirements

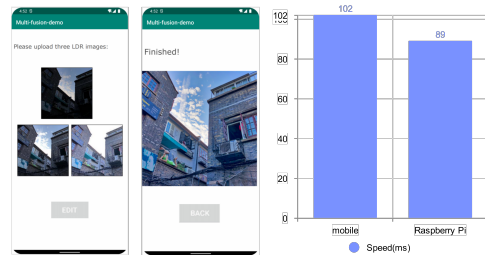


Fig. 9. Results of the program in the Android studio environment.

of mobile devices. In addition, Table I shows the number of parameters for our proposed method and others. We used the API interface provided by PyTorch mobile to embed the quantized model into the Android development program and experimented with the Pixel 4 XL API 32 virtual machine in Android Studio. Some of the experimental results are shown in Figure 9.

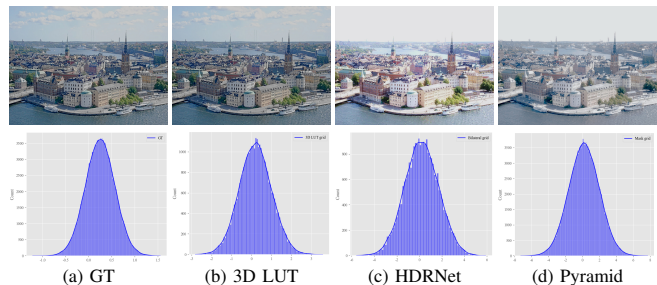


Fig. 10. This figure shows the reconstruction results of the networks and the data distribution of the corresponding grids.



Fig. 11. This figure shows the results of using randomly initialized 3D LUTs (RI) instead of the basic 3D LUTs.

V. DISCUSSION

Why we chose 3D LUT to model multi-exposure image fusion with UHD resolution rather than bilateral learning or pyramids? We conduct two comparison experiments where they (3D LUT, HDRNet, Laplace Pyramid) are performed on a degraded UHD image to obtain a high-quality UHD image. These networks are fine-tuned on the MIT-Adobe FiveK dataset. They are optimized by an AdamW optimizer with an initial learning rate of $1e-3$ and a decay rate of 0.1, we set $\beta_1 = 0.9$, $\beta_2 = 0.999$ and $\varepsilon = 10^{-8}$. We visualize the data distribution of the 3D LUT grid ($32 \times 32 \times 32$), bilateral grid ($12 \times 16 \times 16 \times 8$), and MASK grid ($3 \times 256 \times 256$) (see Figure 10). In general, the data distribution of the grids generated by these networks is close; the mean value of the distribution is almost always around 0.2. However, the variance of each grid is different, and the variance of 3D LUT is the smallest. We assume that this is related to a priori knowledge and remove the basic 3D LUTs and replace them with a fixed distribution grid. The results demonstrate that the

variance of the grid becomes larger ($[-3, 3] \rightarrow [-5, 5]$) and the reconstruction of the image is degraded (see Figure 11).

VI. CONCLUSION

In this paper, we propose a teacher-student network based on a 3D LUT to achieve real-time (33fps) UHD multi-exposure image fusion on a single GPU. In addition, we develop an editable pattern to obtain HDR images of different quality to adapt to different scenes. We discuss the reasons for using 3D LUTs by trading off the two aspects of speed (ms) and accuracy (PSNR). Extensive experimental results validate the effectiveness of our method. Note that the reconstruction effect is not significant for 3D LUTs with grid scales larger than 64.

REFERENCES

- [1] Jianrui Cai, Shuhang Gu, and Lei Zhang. Learning a deep single image contrast enhancer from multi-exposure images. *TIP*, 2018, 4, 8
- [2] Xin Deng, Yutong Zhang, Mai Xu, Shuhang Gu, and Yiping Duan. Deep coupled feedback network for joint exposure fusion and image super-resolution. *TIP*, 2021, 6
- [3] Alexey Dosovitskiy, Lucas Beyer, Alexander Kolesnikov, Dirk Weissenborn, Xiaohua Zhai, Thomas Unterthiner, Mostafa Dehghani, Matthias Minderer, Georg Heigold, Sylvain Gelly, Jakob Uszkoreit, and Neil Houlsby. An image is worth 16x16 words: Transformers for image recognition at scale. In *ICLR*, 2021, 4
- [4] Songtao He, Mohammad Amin Sadeghi, Sanjay Chawla, Mohammad Alizadeh, Hari Balakrishnan, and Samuel Madden. Inferring high-resolution traffic accident risk maps based on satellite imagery and gps trajectories. In *ICCV*, 2021, 3
- [5] Justin Johnson, Alexandre Alahi, and Li Fei-Fei. Perceptual losses for real-time style transfer and super-resolution. In *ECCV*, 2016, 4
- [6] Hakki Can Karaimer and Michael S Brown. A software platform for manipulating the camera imaging pipeline. In *ECCV*, 2016, 3
- [7] Sang-hoon Lee, Jae Sung Park, and Nam Ik Cho. A multi-exposure image fusion based on the adaptive weights reflecting the relative pixel intensity and global gradient. In *ICIP*, 2018, 2
- [8] Fangya Li, Ruipeng Gang, Chenghua Li, Jinjing Li, Sai Ma, Chenming Liu, and Yizhen Cao. Gamma-enhanced spatial attention network for efficient high dynamic range imaging. In *CVPR*, 2022, 1
- [9] Hui Li, Kede Ma, Hongwei Yong, and Lei Zhang. Fast multi-scale structural patch decomposition for multi-exposure image fusion. *TIP*, 2020, 2
- [10] Hui Li and Lei Zhang. Multi-exposure fusion with cnn features. In *ICIP*, 2018, 1
- [11] Jinyuan Liu, Jingjie Shang, Risheng Liu, and Xin Fan. Halder: Hierarchical attention-guided learning with detail-refinement for multi-exposure image fusion. In *ICME*, 2021, 8
- [12] Jinyuan Liu, Jingjie Shang, Risheng Liu, and Xin Fan. Attention-guided global-local adversarial learning for detail-preserving multi-exposure image fusion. *IEEE Transactions on Circuits and Systems for Video Technology*, 2022, 8
- [13] Zhen Liu, Wenjie Lin, Xinpeng Li, Qing Rao, Ting Jiang, Mingyan Han, Haoqiang Fan, Jian Sun, and Shuaicheng Liu. Adnet: Attention-guided deformable convolutional network for high dynamic range imaging. In *CVPR*, 2021, 7, 8
- [14] Jun Luo, Wenqi Ren, Xinwei Gao, and Xiaochun Cao. Multi-exposure image fusion via deformable self-attention. *IEEE TIP*, 32:1529–1540, 2023, 1
- [15] Feifan Lv, Yu Li, and Feng Lu. Attention guided low-light image enhancement with a large scale low-light simulation dataset. *IJCV*, 2021, 4
- [16] Kede Ma, Zhengfang Duanmu, Hojatollah Yeganeh, and Zhou Wang. Multi-exposure image fusion by optimizing a structural similarity index. *IEEE Transactions on Computational Imaging*, 2017, 2
- [17] Kede Ma and Zhou Wang. Multi-exposure image fusion: A patch-wise approach. In *ICIP*, 2015, 2
- [18] Shawn Mathew, Saad Nadeem, Sruti Kumari, and Arie E. Kaufman. Augmenting colonoscopy using extended and directional cyclegan for lossy image translation. In *CVPR*, 2020, 4
- [19] Kangfu Mei, Aiwen Jiang, Juncheng Li, and Mingwen Wang. Progressive feature fusion network for realistic image dehazing. In *ACCV*, pages 203–215, 2018, 3
- [20] Quan H. Nguyen and William J. Beksi. Single image super-resolution via a dual interactive implicit neural network. In *WACV*, 2023, 2
- [21] Eduardo Pérez-Pellitero, Sibi Catley-Chandar, Richard Shaw, Ales Leonardis, Radu Timofte, Zexin Zhang, Cen Liu, Yunbo Peng, Yue Lin, Gaocheng Yu, Jin Zhang, Zhe Ma, Hongbin Wang, Xiangyu Chen, Xintao Wang, Haiwei Wu, Lin Liu, Chao Dong, Shiantao Zhou, Qingsen Yan, Song Zhang, Weiye Chen, Yuhang Liu, Zhen Zhang, Yanning Zhang, Javen Qinfeng Shi, Dong Gong, Dan Zhu, Mengdi Sun, Guannan Chen, Yang Hu, Haowei Li, Baozhu Zou, Zhen Liu, Wenjie Lin, Ting Jiang, Chengzhi Jiang, Xinpeng Li, Mingyan Han, Haoqiang Fan, Jian Sun, Shuaicheng Liu, Juan Marín-Vega, Michael Sloth, Peter Schneider-Kamp, Richard Röttger, Chunyang Li, Long Bao, Gang He, Ziyao Xu, Li Xu, Gen Zhan, Ming Sun, Xing Wen, Junlin Li, Jinjing Li, Chenghua Li, Ruipeng Gang, Fangya Li, Chenming Liu, Shuang Feng, Fei Lei, Rui Liu, Junxiang Ruan, Tianhong Dai, Wei Li, Zhan Lu, Hengyan Liu, Peian Huang, Guangyu Ren, Yonglin Luo, Chang Liu, Qiang Tu, Sai Ma, Yizhen Cao, Steven Tel, Barthelemy Heyrman, Dominique Ginhac, Chul Lee, Gahyeon Kim, Seonghyun Park, An Gia Vien, Truong Thanh Nhat Mai, Howoon Yoon, Tu Vo, Alexander Holston, Sheir Zaheer, and Chan Y. Park. NTIRE 2022 challenge on high dynamic range imaging: Methods and results. In *CVPRW*, 2022, 4
- [22] Linhao Qu, Shaolei Liu, Manning Wang, and Zhijian Song. Transmef: A transformer-based multi-exposure image fusion framework using self-supervised multi-task learning. 2022, 1
- [23] K Ram Prabhakar, V Sai Srikar, and R Venkatesh Babu. Deepfuse: A deep unsupervised approach for exposure fusion with extreme exposure image pairs. In *CVPR*, 2017, 1, 3
- [24] Olaf Ronneberger, Philipp Fischer, and Thomas Brox. U-net: Convolutional networks for biomedical image segmentation. In *MICCAI*, 2015, 3
- [25] Yuda Song, Hui Qian, and Xin Du. Starenhancer: Learning real-time and style-aware image enhancement. In *ICCV*, 2021, 3
- [26] Thomas Verelst and Tinne Tuytelaars. Blockcopy: High-resolution video processing with block-sparse feature propagation and online policies. In *ICCV*, 2021, 3
- [27] Ruixing Wang, Qing Zhang, Chi-Wing Fu, Xiaoyong Shen, Wei-Shi Zheng, and Jiaya Jia. Underexposed photo enhancement using deep illumination estimation. In *CVPR*, 2019, 3
- [28] Tao Wang, Yong Li, Jingyang Peng, Yipeng Ma, Xian Wang, Fenglong Song, and Youliang Yan. Real-time image enhancer via learnable spatial-aware 3d lookup tables. In *ICCV*, 2021, 3
- [29] Haiyan Wu, Yanyun Qu, Shaohui Lin, Jian Zhou, Ruizhi Qiao, Zhizhong Zhang, Yuan Xie, and Lizhuang Ma. Contrastive learning for compact single image dehazing. In *CVPR*, 2021, 3
- [30] Boxue Xiao, Zhuoran Zheng, Xiang Chen, Chen Lv, Yunliang Zhuang, and Tao Wang. Single UHD image dehazing via interpretable pyramid network. 2022, 1
- [31] Han Xu, Jiayi Ma, Junjun Jiang, Xiaojie Guo, and Haibin Ling. U2fusion: A unified unsupervised image fusion network. *TPAMI*, 2020, 8
- [32] Han Xu, Jiayi Ma, Zhuliang Le, Junjun Jiang, and Xiaojie Guo. FusionDn: A unified densely connected network for image fusion. In *AAAI*, 2020, 1
- [33] Han Xu, Jiayi Ma, and Xiao-Ping Zhang. Mef-gan: Multi-exposure image fusion via generative adversarial networks. *TIP*, 2020, 1
- [34] Qingsen Yan, Dong Gong, Qinfeng Shi, Anton van den Hengel, Chunhua Shen, Ian Reid, and Yanning Zhang. Attention-guided network for ghost-free high dynamic range imaging. In *CVPR*, 2019, 7, 8
- [35] Qingsen Yan, Song Zhang, Weiye Chen, Yuhang Liu, Zhen Zhang, Yanning Zhang, Javen Qinfeng Shi, and Dong Gong. A lightweight network for high dynamic range imaging. In *CVPR*, 2022, 1
- [36] Canqian Yang, Meiguang Jin, Yi Xu, Rui Zhang, Ying Chen, and Huaida Liu. Seplut: Separable image-adaptive lookup tables for real-time image enhancement. In *ECCV*, 2022, 3
- [37] Fei Ye and Adrian G. Bors. Lifelong teacher-student network learning. *TPAMI*, 2022, 2
- [38] Gaocheng Yu, Jin Zhang, Zhe Ma, and Hongbin Wang. Efficient progressive high dynamic range image restoration via attention and alignment network. In *CVPRW*, 2022, 1
- [39] Yuhui Yuan, Rao Fu, Lang Huang, Weihong Lin, Chao Zhang, Xilin Chen, and Jingdong Wang. Hrformer: High-resolution transformer for dense prediction. In *NIPS*, 2021, 3
- [40] Hui Zeng, Jianrui Cai, Lida Li, Zisheng Cao, and Lei Zhang. Learning image-adaptive 3d lookup tables for high performance photo enhancement in real-time. *IEEE TPAMI*, 44(4):2058–2073, 2020, 3
- [41] Hui Zeng, Jianrui Cai, Lida Li, Zisheng Cao, and Lei Zhang. Learning image-adaptive 3d lookup tables for high performance photo enhancement in real-time. *TPAMI*, 2022, 1
- [42] Fengyi Zhang, Hui Zeng, Tianjun Zhang, and Lin Zhang. Clut-net:

- Learning adaptively compressed representations of 3dluts for lightweight image enhancement. 2022. [3](#)
- [43] Pengchuan Zhang, Xiyang Dai, Jianwei Yang, Bin Xiao, Lu Yuan, Lei Zhang, and Jianfeng Gao. Multi-scale vision longformer: A new vision transformer for high-resolution image encoding. *arXiv preprint arXiv:2103.15358*, 2021. [3](#)
- [44] Yu Zhang, Yu Liu, Peng Sun, Han Yan, Xiaolin Zhao, and Li Zhang. IFCNN: A general image fusion framework based on convolutional neural network. *Information Fusion*, 2020. [1](#)
- [45] Kaiwen Zheng, Jie Huang, Hu Yu, and Feng Zhao. Efficient multi-exposure image fusion via filter-dominated fusion and gradient-driven unsupervised learning. In *CVPRW*, 2023. [1](#)
- [46] Zhuoran Zheng, Wenqi Ren, Xiaochun Cao, Tao Wang, and Xiuyi Jia. Ultra-high-definition image HDR reconstruction via collaborative bilateral learning. In *ICCV*, 2021. [1](#)